Tomasz Raszkowski
Agnieszka Samson

NUMERICAL APPROACHES TO THE HEAT TRANSFER PROBLEM IN MODERN ELECTRONIC STRUCTURES

Abstract

The main aim of this paper is to present a detailed description of the research related to the modeling of heat conduction in modern electronic structures, including special consideration for numerical aspects of analyzed algorithms. The motivation to undertake the research as well as some of the most-important results of the experiments and simulations are also included. Moreover, a numerical approximation of the problem as well as the methodology used and a sample solution of the mentioned problem are presented. In the main part, the discretization techniques, Ordinary Differential Equation algorithms, and simulation results for Runge-Kutta's and Gear's algorithms are analyzed and discussed. Additionally, a new effective approach to the modeling of heat transfer in electronic nanostructures is demonstrated.

1. Introduction

The heat transfer problem comprises one of the most-important elements in creating modern electronic systems. Enhancing the effectiveness of such structures entails an increase of their operating speed. This fact, in turn, results in increased heat generation. So, the ability to calculate microchip temperatures is crucial to the proper functioning of the whole electronic system.

The motivation to undertake this research is related to the proper determination of generated heat inside modern nanoelectronic structures. Nowadays, because of customers demands, electronic devices are becoming smaller, thinner, and faster. This situation causes an increase in heat generation inside these structures and a simultaneous increase in their operating frequency. Most of the currently used thermal simulators are based on the parabolic partial differential equation (with mixed boundary conditions), which is known as the Fourier-Kirchhoff equation [4]. However, for instance, the modeling of temperature distribution in modern nanotransistors in the latest integrated circuits using the previously mentioned approach is not correct [8]. Thus, simulation results based on the Fourier-Kirchhoff model may bear significant errors. Research shows that more than half of electronic failures were caused by a thermal reason [12]. Due to this fact, alternative models are needed that would allow the consideration of the nanoscale effect in heat conduction. Therefore, the analysis of heat transfer problems in nanoelectronic systems is currently one of the most important research areas. Moreover, research results may contribute to an increase in the accuracy of electronic system thermal simulation and further optimization.

Thus, the main aim of the research presented in this paper was to model heat distribution in modern electronics using the newest approaches and advanced numerical methods. The results were compared with outputs yielded using the classical model of heat transfer in microsized structures.

2. Selected thermal model overview

This section presents the classical heat transfer theory that was established by Jean-Baptiste Joseph Fourier in 1822 [4]. This theory was based on a heat conduction law, which is also called the Fourier's law. This law can be formulated in the following mathematical form:

$$q(x,t) = -k\nabla T(x,t), \qquad \text{for} \quad x \in \mathbb{R}, \quad t \in \mathbb{R}_+ \cup \{0\}, \tag{1}$$

where:
- q means the local heat flux density,
- k means the material conductivity characterized for analyzed material,
- T means the temperature,
- ∇T means the gradient of the temperature,
- x is the location variable,
- t is the time variable.

The law described above states that the temperature gradient is proportional to the negative heat flux. It is worth highlighting that the negative sign on the right side of the equation describing Fourier's law indicates that the heat propagate from the warmer areas towards the cooler ones.

Fourier's law contributed to the formulation of the parabolic partial differential Fourier-Kirchhoff equation, which is analyzed with mixed boundary conditions. The differential form of this equation demonstrates that the time derivative of the temperature function is equal to the negative product of the gradient of the heat flux and the reciprocal of the volumetric heat capacity. This can be expressed in the following form:

$$\frac{\partial T(x,t)}{\partial t} = -\frac{1}{c_{vs}} \nabla q(x,t), \qquad \text{for} \quad x \in \mathbb{R}, \quad t \in \mathbb{R}_+ \cup \{0\}, \tag{2}$$

where c_{vs} means the volumetric heat capacity.

Both the Fourier-Kirchhoff formula and Fourier's law have had a significant influence on the classical approach to modeling heat conduction in solid states, because they have established the classical heat transfer theory. This theory has been applied to temperature determination for a very long time, since the early twenties of the 19th Century until almost the end of the 20th. The Fourier-Kirchhoff theory has helped establish a satisfying description of thermal processes occurring in relatively large structures and when thermal analyses times are relatively long.

Regrettably, the Fourier-Kirchhoff theory imposes few assumptions that are not in accordance with commonly known and proven physical theories. One of behaviors that seems to be non-physical is the infinite speed of the propagation of heat. Another non-physical presumption concerns the investigated Fourier-Kirchhoff equation, which states that the heat flux as well as the temperature gradient are able to instantaneously change, which does not agree with empirical research [5, 6]. In addition, owing to the miniaturization of many electronic devices and the influential speed gain of their operation, the Fourier-Kirchhoff model is not apposite for electronic structures developed in technology nodes smaller than about 200 nm [8]. This is a very important issue due to the development of the MOSFET manufacturing technology. These kinds of nanosized transistors are used, for example, in the newest Intel Broadwell CPUs designed in 14 nm technology node as well as some other smaller ones such as the prototypical Fin-FET nanotransistors developed in 6 nm technology node, nanotube, or nanowire manufacturing technology [14].

Consequently, there is a significant need for some other thermal approaches that are able to include considerations related to the microsized effects in thermal models. There are some mathematical models that are congruent for heat transfer modeling in nanosized structures. The most popular of these are listed below:

- Boltzmann Transport Equation model (BTE),
- Molecular Dynamics model (MD),
- Schrödinger Equation model (SE),

- Ballistic-Diffusive Equation model (BDE),
- Dual-Phase-Lag model (DPL).

The first model, listed above, is the Boltzmann Transport Equation [2]. This model was developed in the 1870s by Ludwig Boltzmann, an Austrian physicist. This model can be applied in realistic electronic structures that are designed in nanoscale. Their node size can be equal to a few nanometers. The applicability of the above-mentioned model is also dedicated for much larger structures, even up to hundreds of nanometers.

The second model, mentioned in the list above, is based on molecular dynamics research [2]. This can be applied to very tiny structures, even for structures whose technology node is not much larger than 1 nm. This mathematical model was established in the 1950s. Initially, it was designated for biomolecules modeling only; for example, in chemical physics or some material sciences.

The next model, called the Schrödinger Equation model, is also appropriate for thermal modeling in nanosized structures. It is based on the Schrödinger Equation. This model was delivered and announced in the 1920s. Its originator was Erwin Schrödinger, an Austrian physicist. The equation formulated by Schrödinger reflects changes that occur in the quantum states of physical systems over time. The Schrödinger Equation model could also be applied to structures developed in technology markedly smaller than 1 nm. This makes it possible taking into consideration structures that are smaller than the parameter of the silicon lattice.

Another model, adequate for thermal modeling in nanometric structures, is the Ballistic-Diffusive Equation model. The history of this model reaches the beginning of the 21st Century. It was established by G. Chen [3]. Similar to the Boltzmann Transport Equation,the investigated model is dedicated to electronic structures that are manufactured in about the 100 nm technology node.

Despite the fact that all of the mentioned heat transfer models are applicable in the case of nanometric structures, the simulations that use them are characterized by huge computational complexity. Thus, the simulations demand plenty of time. This fact causes many inconveniences in the applicability of each of these models.

Therefore, another mathematical model apposite for the modeling of heat transfer at the nanoscale will be taken into consideration. This model is called the Dual-Phase-Lag model; it was delivered in the mid-1990s by Da Yu Tzou [15]. This is a very useful mathematical model that allows for both the parabolic and the hyberbolic heat transfer models. Thus, it can be successfully used instead of the Fourier-Kirchhoff model. Furthermore, the Dual-Phase-Lag model is suitable for the modeling of heat transfer in many microscopic and nanosized electronic structures, even in those that are developed in technology nodes smaller than 200 nm and that operate at frequencies exceeding 6 GHz [17]. Moreover, the empirical confirmation that the heat transfer in nanosized structures (especially in one-dimensional structures) can be described using the Dual-Phase-Lag model is presented in [11]. The Dual-Phase-Lag model will be discussed in detail in the next chapter.

An approximate scope of the applicability of the heat transfer models mentioned in this paragraph are marked in Figure 1.
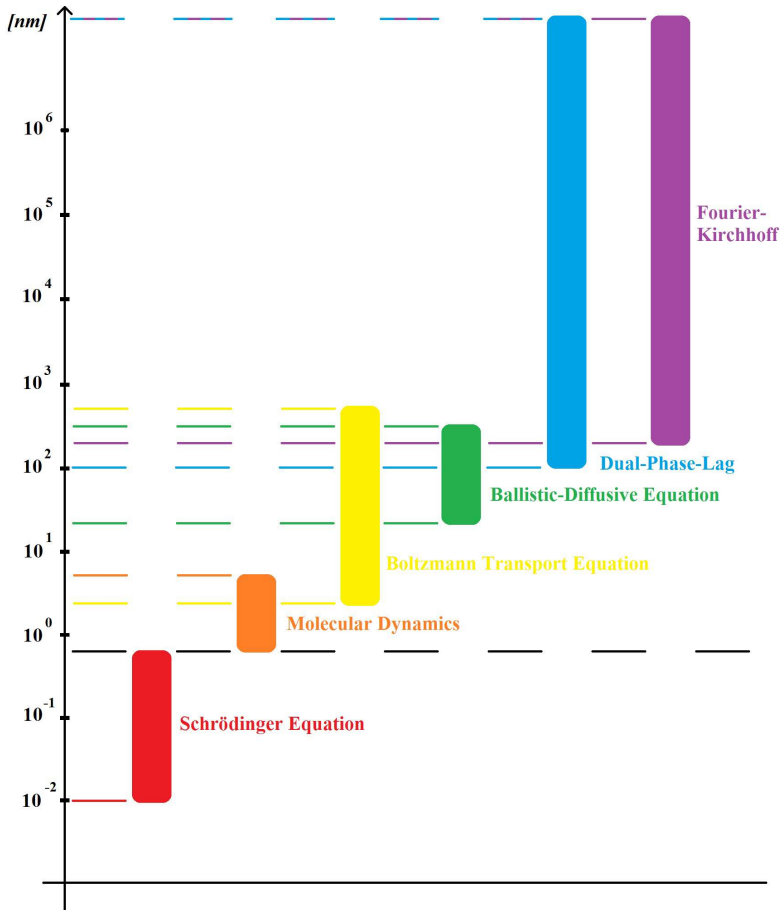

Figure 1. An approximate scope of the applicability of the heat transfer models.

3. Dual-Phase-Lag thermal model

The Dual-Phase-Lag model will be presented in this section. This model was used to determine temperature distribution in a chosen structure. The Dual-Phase-Lag model was based on the classical Fourier-Kirchhoff equation, but some very important modifications were made. These modifications were effectuated in order to adapt classical theory to the newest technology based on very small transistors that are produced in technology nodes down to several dozen nanometers and operate at very high frequencies.

The principal change is associated with the introduction of two new variables. Each of them includes the time lag which is observed in the case of heat propagation as well as the temperature response. These two time lags explain the name of the investigated model. This thermal model, including the mentioned time lags, can be expressed (for example) in the form of a system of equations, presented as follows [16]:

$$
\begin{cases}
\nabla q(x,t) &= -c_{vs}\dfrac{\partial T(x,t)}{\partial t} \\
k \cdot \tau_T \dfrac{\partial \nabla T(x,t)}{\partial t} + \tau_q \dfrac{\partial q(x,t)}{\partial t} &= -k \cdot \nabla T(x,t) - q(x,t)
\end{cases}
\tag{3}
$$

where:

$$
x \in \mathbb{R}, \quad t \in \mathbb{R}_+ \cup \{0\}.
$$

Quantities that appear in the bottom equation in the system of equations above have the following meanings:
- k is the thermal conductivity,
- τ_q is the time lag of the heat flux,
- τ_T is the time lag of the temperature.

Quantity k is also known as the measure of the ratio of the heat conduction.

It is worth saying that, in the case of the τ_T variable being equal to 0, the described Dual-Phase-Lag model remolds to the Cattaneo-Vernotte model [10]. This situation indicates the hyperbolic character of the heat transfer equation.

On the other hand, when quantities τ_q and τ_T are equal to 0, the Dual-Phase-Lag model is translated into the original form of the classical Fourier's law.

Furthermore, when thermal conductivity does not depend on the temperature (and in the case of a lack of internal heat generation), the Dual-Phase-Lag equation can be briefly expressed in the following form [10]:

$$
\alpha \left(\tau_T \frac{\partial \nabla^2 T(x,t)}{\partial t} + \nabla^2 T(x,t) \right) - \frac{\partial T(x,t)}{\partial t} - \tau_q \frac{\partial^2 T}{\partial t^2} = 0.
\tag{4}
$$

where:

$$
\alpha = \frac{k}{c_{vs}}.
\tag{5}
$$

Parameter α in the relation presented above is called the thermal diffusivity.

In contrast to the hyperbolic heat conduction models, the model presented above contains the mixed space and time derivative of the third order. Moreover, when temperature time lag τ_T and heat flux time lag τ_q are equal to 0, the last Dual-Phase-Lag equation form is reduced to the Fourier-Kirchhoff equation presented in the previous section of this paper.

4. Methodology and proposed algorithm

One of the first steps in the research was to properly describe the heat flux in selected structure. A silicon slab with a thickness of 10 nm was chosen. Its lateral dimensions

were significantly greater than its thickness. One problem concerned the modeling of the heat flux along the benchmark structure. It was decided that the initial research would include the one-dimensional case, which pertained the slab thickness only. That slab was heated from one side and perfectly cooled from the other. Figure 2 presents the described silicon structure.
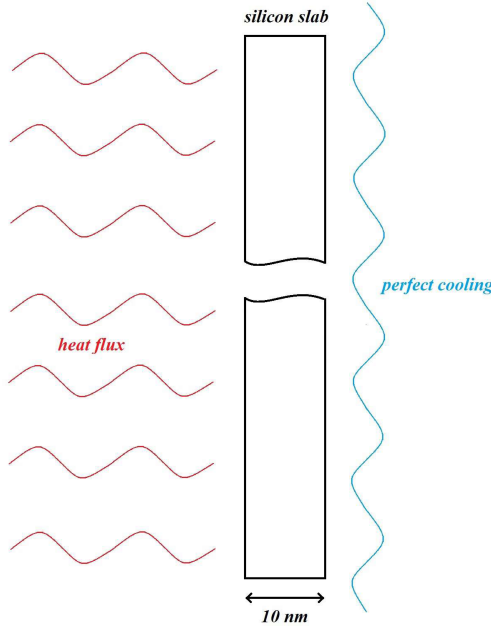

Figure 2. The one-dimensional benchmark structure.

The presented approach concerns the Finite Difference Method usage. As mentioned earlier, in the case of the nanoscale, the description of the heat transfer behavior can be obtained using the Dual-Phase-Lag model that was presented in the previous section. This problem was solved with the following initial conditions:

$$T(x,t)|_{t=0} = 0 \quad \text{for} \quad x \in (0, L), \tag{6}$$

where L means the thickness of the considered silicon slab. Moreover, the following boundary conditions have been imposed:

$$q(x,t)|_{x=0} = a \cdot \mathbf{1}(t) \quad \text{for} \quad t \in \mathbb{R}_+ \cup \{0\}, \quad a \in \mathbb{R}, \tag{7}$$

and

$$T(x,t)|_{x=L} = 0 \quad \text{for} \quad t \in \mathbb{R}_+ \cup \{0\}. \tag{8}$$

In order to obtain a numerical solution, the Finite Difference Method was used. The discretization mesh of the considered problem can be performed in graphical form, as seen in Figure 3.
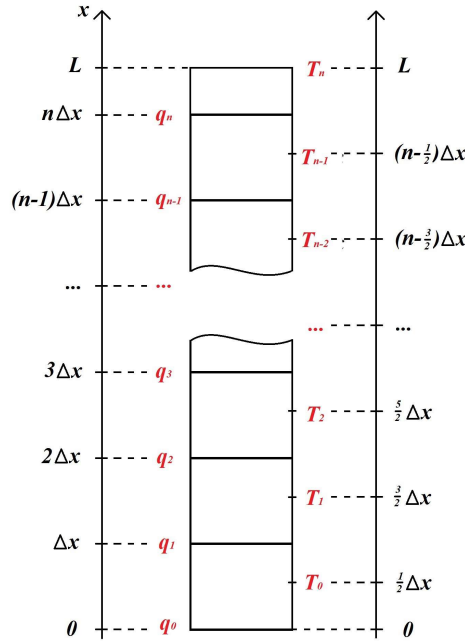
Figure 3. The Finite Difference Method discretization mesh.

The analytical form of the presented discretization mesh presents as follows:

$$T_i = T(x,t)|_{x=\left(i+\frac{1}{2}\right)\cdot\Delta x} \quad \text{for} \quad i = 0, 1, 2, \ldots, n-1, \tag{9}$$

$$T_n = T(x,t)|_{x=L} \tag{10}$$

and

$$q_i = q(x,t)|_{x=i\cdot\Delta x} \quad \text{for} \quad i = 0, 1, 2, \ldots, n. \tag{11}$$

The solution was received using the Finite Difference equations presented below:

$$\begin{bmatrix} T_0' \\ T_1' \\ T_2' \\ \vdots \\ T_{n-2}' \\ T_{n-1}' \end{bmatrix} = \frac{-1}{c_{vs}\cdot\Delta x}\cdot\begin{bmatrix} -1 & 0 & 0 & 0 & 0 & 0 \\ 1 & -1 & 0 & 0 & 0 & 0 \\ 0 & 1 & -1 & 0 & 0 & 0 \\ \ddots & \ddots & \ddots & \ddots & \ddots & \ddots \\ 0 & 0 & 0 & 1 & -1 & 0 \\ 0 & 0 & 0 & 0 & 1 & -1 \end{bmatrix}\cdot\begin{bmatrix} q_1 \\ q_2 \\ q_3 \\ \vdots \\ q_{n-1} \\ q_n \end{bmatrix} + \begin{bmatrix} \frac{q_0(t)}{c_{vs}\cdot\Delta x} \\ 0 \\ 0 \\ \vdots \\ 0 \\ 0 \end{bmatrix} \tag{12}$$

and

$$
\begin{bmatrix} q'_1 \\ q'_2 \\ q'_3 \\ \vdots \\ q'_{n-1} \\ q'_n \end{bmatrix} = -\frac{1}{\tau_q} \cdot \begin{bmatrix} q_1 \\ q_2 \\ q_3 \\ \vdots \\ q_{n-1} \\ q_n \end{bmatrix} + \frac{k}{\tau_q \cdot \Delta x} \cdot \begin{bmatrix} 1 & -1 & 0 & 0 & 0 & 0 \\ 0 & 1 & -1 & 0 & 0 & 0 \\ 0 & 0 & 1 & -1 & 0 & 0 \\ \ddots & \ddots & \ddots & \ddots & \ddots & \ddots \\ 0 & 0 & 0 & 0 & 1 & -1 \\ 0 & 0 & 0 & 0 & 0 & 1 \end{bmatrix} \cdot \begin{bmatrix} T_0 \\ T_1 \\ T_2 \\ \vdots \\ T_{n-2} \\ T_{n-1} \end{bmatrix} +
$$

$$
+ \frac{k \cdot \tau_T}{\tau_q \cdot \Delta x} \cdot \begin{bmatrix} 1 & -1 & 0 & 0 & 0 & 0 \\ 0 & 1 & -1 & 0 & 0 & 0 \\ 0 & 0 & 1 & -1 & 0 & 0 \\ \ddots & \ddots & \ddots & \ddots & \ddots & \ddots \\ 0 & 0 & 0 & 0 & 1 & -1 \\ 0 & 0 & 0 & 0 & 0 & 1 \end{bmatrix} \cdot \begin{bmatrix} T'_0 \\ T'_1 \\ T'_2 \\ \vdots \\ T'_{n-2} \\ T'_{n-1} \end{bmatrix}, \tag{13}
$$

where variables with apostrophes denote the time derivatives. Moreover:

$$
T'_n = 0 \tag{14}
$$

and

$$
q_0(t) = a \cdot \mathbf{1}(t) \quad \text{for} \quad a \ \in \mathbb{R}. \tag{15}
$$

5. Simulation results

The simulations using the proposed Finite Difference Method were conducted in the Matlab environment. The solution was obtained by employing an algorithm that was prepared especially for this reason. Moreover, some numerical methods that allow us to solve ordinary differential equations have been used. Among others, the Runge-Kutta formulas and Gear's method were very helpful. The Runge-Kutta methods have been chosen for the analyzed stiff problem due to their strong stability-preserving properties. On the other hand, Gear's method has been employed because it is characterized by A-stability behavior. Apart from that, the following values of silicon material parameters were used:

$$
c_{vs} = 1780 \frac{\text{kJ}}{\text{K} \cdot \text{m}^3}, \quad k = 0.16 \frac{\text{kW}}{\text{K} \cdot \text{m}}, \quad \tau_q = 3 \cdot 10^{-12}\text{s}, \quad L = 10\text{nm}.
$$

Simulations were carried out for different number of the discretization mesh nodes n. Additionally, dimensionless parameter B (defined as ratio $\frac{\tau_T}{2 \cdot \tau_q}$) was harnessed. This parameter allows us to control the transition between various behaviors of heat conduction. The experiments show that the value of parameter B determines three cases [1].

1. The Fourier-Kirchhoff solution when $B = 0.5$.

Part I: $\tau_T = \tau_q = 0$. In this case, parameter B is not formally defined as ratio $\frac{\tau_T}{2 \cdot \tau_q}$. However, assuming that $\tau_T = \tau_q = 0$, using equations (4) and (5), the following formula was obtained:

$$\frac{k}{c_{vs}} \nabla^2 T(x,t) = \frac{\partial T(x,t)}{\partial t}. \tag{16}$$

Using algebraic transformations, the following equation was written:

$$-\nabla \left(-k\nabla T(x,t)\right) = c_{vs} \frac{\partial T(x,t)}{\partial t}. \tag{17}$$

Finally, using Fourier's law, the Fourier-Kirchhoff equation was obtained:

$$-\nabla q(x,t) = c_{vs} \frac{\partial T(x,t)}{\partial t}. \tag{18}$$

Part II: $\tau_T = \tau_q = \tau, \tau > 0$. Using equations (4) and (5) and assuming that $\tau_T = \tau_q = \tau > 0$, the following formula was obtained:

$$\frac{k}{c_{vs}} \left(\tau \frac{\partial \nabla^2 T(x,t)}{\partial t} + \nabla^2 T(x,t) \right) - \frac{\partial T(x,t)}{\partial t} - \tau \frac{\partial^2 T}{\partial t^2} = 0. \tag{19}$$

Using basic algebraic transformations, the following expression was fulfilled:

$$c_{vs} \frac{\partial T(x,t)}{\partial t} = -\tau \frac{\partial}{\partial t} \left(c_{vs} \frac{\partial T(x,t)}{\partial t} \right) + \nabla \left(k\nabla T(x,t) \right) + \nabla \left(k\tau \frac{\partial \nabla T(x,t)}{\partial t} \right). \tag{20}$$

Knowing that expression (2) is fulfilled, the considered equation (20) was transformed into the following formula:

$$c_{vs} \frac{\partial T(x,t)}{\partial t} = -\tau \frac{\partial}{\partial t} \left(-\nabla q(x,t) \right) + \nabla \left(k\nabla T(x,t) \right) + \nabla \left(k\tau \frac{\partial \nabla T(x,t)}{\partial t} \right). \tag{21}$$

After some algebraic transformations, the following equation was written:

$$c_{vs} \frac{\partial T(x,t)}{\partial t} = \nabla \left(\tau \frac{\partial q(x,t)}{\partial t} + k\nabla T(x,t) + k\tau \frac{\partial \nabla T(x,t)}{\partial t} \right). \tag{22}$$

Using expression (2) again, the formula below was yielded:

$$-\nabla q(x,t) = \nabla \left(\tau \frac{\partial q(x,t)}{\partial t} + k\nabla T(x,t) + k\tau \frac{\partial \nabla T(x,t)}{\partial t} \right). \tag{23}$$

Hence, the succeeding formula was determined:

$$q(x,t) + \tau \frac{\partial q(x,t)}{\partial t} = -k\nabla T(x,t) - k\tau \frac{\partial \nabla T(x,t)}{\partial t}. \tag{24}$$

Using the approximation mentioned in [13], the formula above can be written in the following form:

$$q(x, t + \tau) = -k\nabla T(x, t + \tau). \tag{25}$$

Substituting $s = t + \tau$, Fourier's law was obtained:

$$q(x, s) = -k\nabla T(x, s), \tag{26}$$

which finally leads to the formulation of the Fourier-Kirchhoff equation.

2. **The hyperbolic solution when $B \to 0$.**

Considering that $B = \frac{\tau_T}{2\tau_q} \to 0$, it can be assumed that $\tau_T \to 0$, or that the value of parameter τ_T is significantly smaller than the value of parameter τ_q. Thus, parameter τ_T can be neglected. Then, the Dual-Phase-Lag equation can be written in the form presented below:

$$-\alpha\nabla^2 T(x, t) + \frac{\partial T(x, t)}{\partial t} + \tau_q \frac{\partial^2 T(x, t)}{\partial t^2} = 0. \tag{27}$$

However, considering the one-dimensional case, this equation can be rewritten in the following form:

$$-\alpha\frac{\partial^2 T(x, t)}{\partial x^2} + \frac{\partial T(x, t)}{\partial t} + \tau_q \frac{\partial^2 T(x, t)}{\partial t^2} = 0. \tag{28}$$

Using the classical theory of partial differential equations, the expression above can be formulated as:

$$A\mu_{xx} + B\mu_{xt} + C\mu_{tt} + D\mu_x + E\mu_t + F\mu = f, \tag{29}$$

where:

$$\mu_{xx} = \frac{\partial^2 T(x, t)}{\partial x^2}, \quad \mu_{xt} = \frac{\partial^2 T(x, t)}{\partial x \partial t}, \quad \mu_{tt} = \frac{\partial^2 T(x, t)}{\partial t^2},$$

$$\mu_x = \frac{\partial T(x, t)}{\partial x}, \quad \mu_t = \frac{\partial T(x, t)}{\partial t}, \quad \mu = T(x, t),$$

$$f = 0 \quad for \quad x \in \mathbb{R}, \quad t \in \mathbb{R}_+ \cup \{0\},$$

$$A = -\alpha, \quad B = 0, \quad C = \tau_q, \quad D = 0, \quad E = 1, \quad F = 0.$$

The simplified form of the previous equation presents as follows:

$$-\alpha\mu_{xx} + \tau_q\mu_{tt} + \mu_t = 0, . \tag{30}$$

The character of the partial differential equation of the second order presented above can be determined by calculating the value of the following discriminant:

$$\Delta(x, t) = B^2 - 4AC, \tag{31}$$

which means that, in the considered case, this value is equal to:

$$\Delta(x,t) = 0^2 - 4\left(-\alpha\right)\tau_q = \frac{4k\tau_q}{c_{vs}} > 0. \tag{32}$$

The positive value of the discriminant above indicates that the analyzed equation has hyperbolic behavior.

3. **The heat transfer that is characteristic, for example, for nanosized metals, when $B \gg 0.5$.**

When the value of parameter B is greater than 0.5, the heat diffusion speed is also greater than the one that is determined by the classical Fourier theory [7]. On the other hand, when the value of the mentioned parameter B is smaller than 0.5 (hyperbolic case), the generated heat diffuses more slowly than predicted in the case of the Fourier theory. It is also worth saying that the heat transfer described by the hyperbolic equation will not be a main research task in the future.

In further analyses, time variables and coordinates will be presented in normalized forms in order to make mathematical analyses more convenient and allow comparisons of the different approaches to the heat transfer problem. Normalization formulas were determined as follows:

$$x^N = \frac{x}{L} \tag{33}$$

and

$$T^N = \frac{T}{T_{max}}. \tag{34}$$

Parameter T_{max} means maximal steady-state temperature, and it is expressed in the following form:

$$T_{max} = \frac{q \cdot L}{k}. \tag{35}$$

A brief comparison of the results obtained in the presented way when parameter $B = 0.5$ and others that have been yielded using Green's functions for the Fourier-Kirchhoff equation and described in [9] is demonstrated in Figure 4.

It is easy to see that, in the foregoing figure, the normalized values of the temperature observed alongside the investigated structure are presented. Each couple of colorful and their corresponding black curves demonstrate the distribution of the temperature observed at different time instants. The black curves show the results that have been obtained based on the Fourier-Kirchhoff equation. On the other hand, the cyan, magenta, green, and blue curves indicate the outputs yielded using the Dual-Phase-Lag equation for 4 fs, 40 fs, 400 fs, and 4000 fs, respectively. Moreover, in order to make the analysis more convenient, the horizontal axis is described using

a logarithmic scale. As can be seen, each mentioned color and its corresponding black curve coincide with each other. Hence, both the Fourier-Kirchhoff and Dual-Phase-Lag (for $B = 0.5$) methods produce exactly the same results, so this denotes the correctness of the proposed scheme.
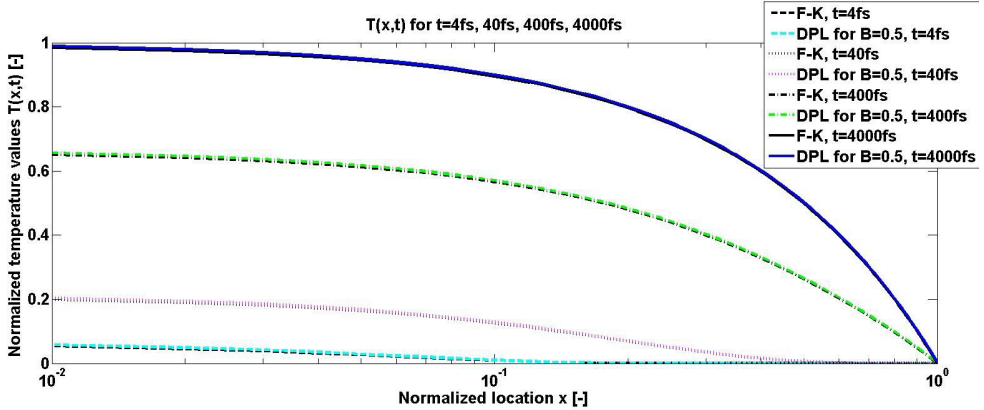

Figure 4. Comparison of the Fourier-Kirchhoff and Dual-Phase-Lag models for $B = 0.5$.

The temperature solutions yielded using the Fourier-Kirchhoff model or, equivalently, using the Dual-Phase-Lag model when parameter $B = 0.5$ and solutions based on the Dual-Phase-Lag model for $B = 0.3$ are presented in Figure 5. The mentioned figure above demonstrates that the temperature solutions received using the Dual-Phase-Lag model for parameter $B = 0.3$, representing the hyperbolic model and marked by dashed curves, overestimates the values of the temperatures in the heat source and its surroundings. However, a higher value of average surface temperature is observed using the Fourier-Kirchhoff equation (which is marked by the solid curves). In Figure 5, the results obtained for different time instants are presented. Time instants are equal to 4 fs, 40 fs, 400 fs, and 4000 fs, respectively. Similar to the previous figure, the horizontal axis is described using a logarithmic scale.

On the other hand, Figure 6 shows the temperature distribution received using, again, the Fourier-Kirchhoff model or, equivalently, the Dual-Phase-Lag model when parameter $B = 0.5$. Moreover, temperature distribution based on the Dual-Phase-Lag model when $B = 7$ is also shown.

In the case when $B > 0.5$, the speed of heat diffusion is initially larger than the heat diffusion speed observed using the Fourier-Kirchhoff equation. Similar to Figure 5, the normalized distribution of temperature is presented in Figure 6. The temperature distribution is demonstrated for 4 fs, 40 fs, 400 fs, and 4000 fs, respectively. Like in the previous cases, the horizontal axis is described using a logarithmic scale to make the analysis more convenient.

The computational complexity of the investigated algorithm was estimated based on the temperature distribution yielded for different numbers of nodes in the dis-

cretization mesh, different values of parameter B, and all numerical methods presented in the previous section. Moreover, the values of temperature were computed for several time instants. The chosen simulation environment was Matlab. All simulations were supported by an Intel® Core™ i7 CPU (2.5 GHz, 3.5 GHz in Intel® Turbo Boost Technology 2.0) with Hyper-Threading Technology (four cores, eight threads), 16 GB RAM DDR3, and the Microsoft Windows operating system (ver. 10). Furthermore, sparse matrices were employed in order to reduce RAM memory and CPU power consumption.
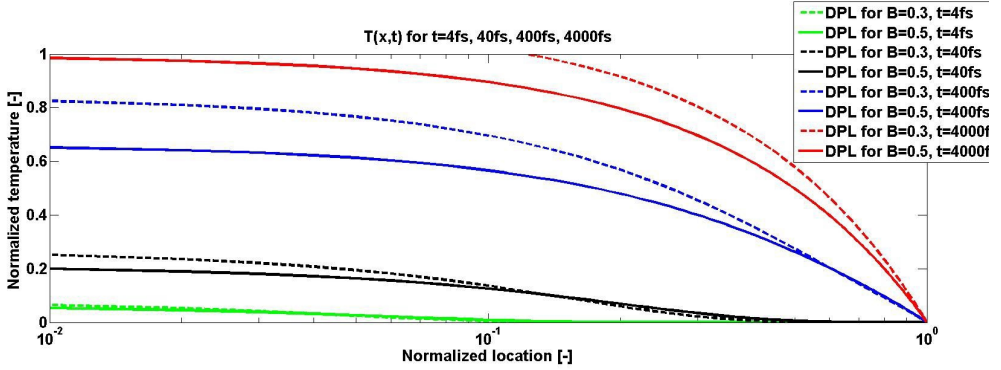

Figure 5. Comparison of temperature solutions for the Fourier-Kirchhoff and Dual-Phase-Lag models for $B = 0.3$.
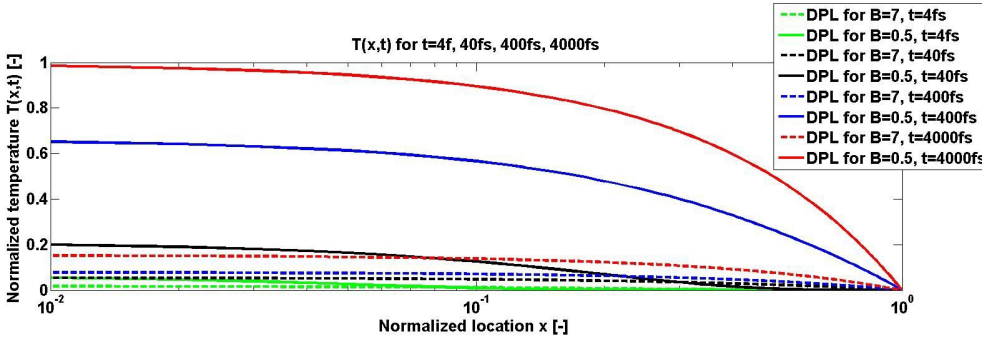

Figure 6. Comparison of temperature solutions for the Fourier-Kirchhoff and Dual-Phase-Lag models for $B = 7$.

Then, the duration of each of the simulations was measured. Their results are clearly visible in Figure 7.

Moreover, the number of temperature function evaluations, multiplication operations, and summation operations for each employed numerical method were counted during the simulation. The comparison of the number of temperature

function evaluations with respect to the number of discretization nodes is presented in Figure 8.
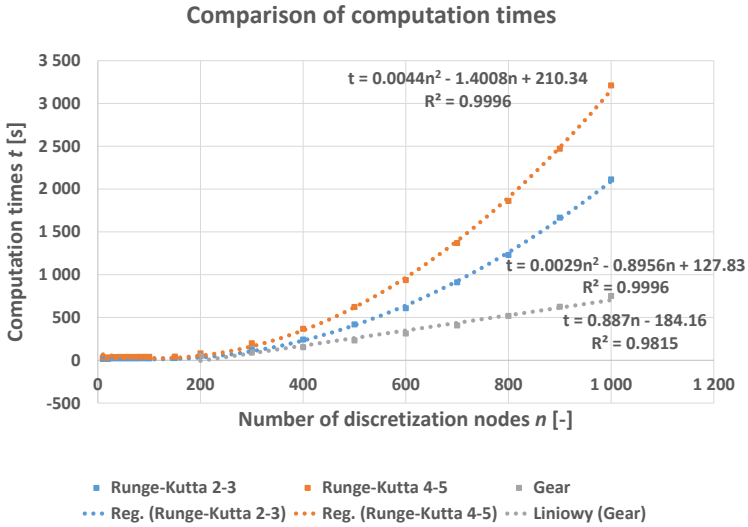
Comparison of computation times

$$t = 0.0044n^2 - 1.4008n + 210.34$$
$$R^2 = 0.9996$$

$$t = 0.0029n^2 - 0.8956n + 127.83$$
$$R^2 = 0.9996$$

$$t = 0.887n - 184.16$$
$$R^2 = 0.9815$$

- Runge-Kutta 2-3
- Runge-Kutta 4-5
- Gear
- Reg. (Runge-Kutta 2-3)
- Reg. (Runge-Kutta 4-5)
- Liniowy (Gear)

Figure 7. Computation time comparison.

Comparison of number of function evaluations

$$n_{eval} = 29.414n^2 - 2101.1n + 566001$$
$$R^2 = 0.9998$$

$$n_{eval} = 17.989n^2 - 1013.6n + 271540$$
$$R^2 = 0.9999$$

- Runge-Kutta 2-3
- Runge-Kutta 4-5
- Gear
- Reg. (Runge-Kutta 2-3)
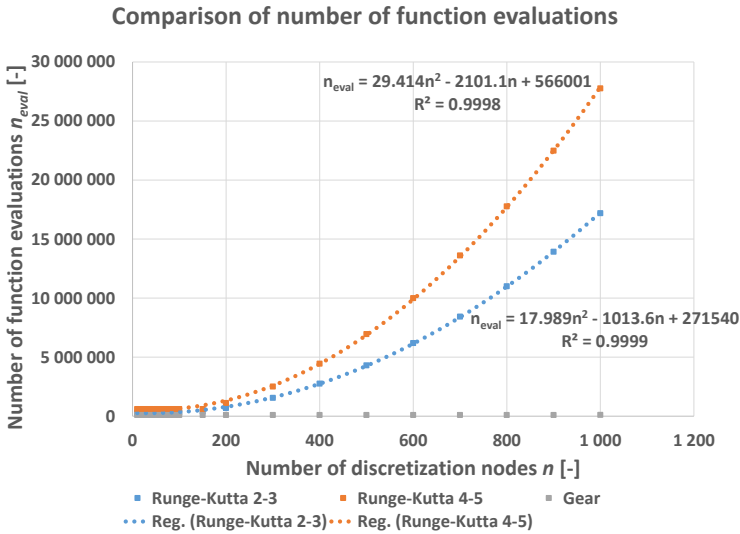- Reg. (Runge-Kutta 4-5)

Figure 8. Comparison of the number of temperature function evaluations.

In order to make analysis easier, the number of temperature function evaluations in Gear's method in relation to the number of the discretization nodes is presented separately in Figure 9.
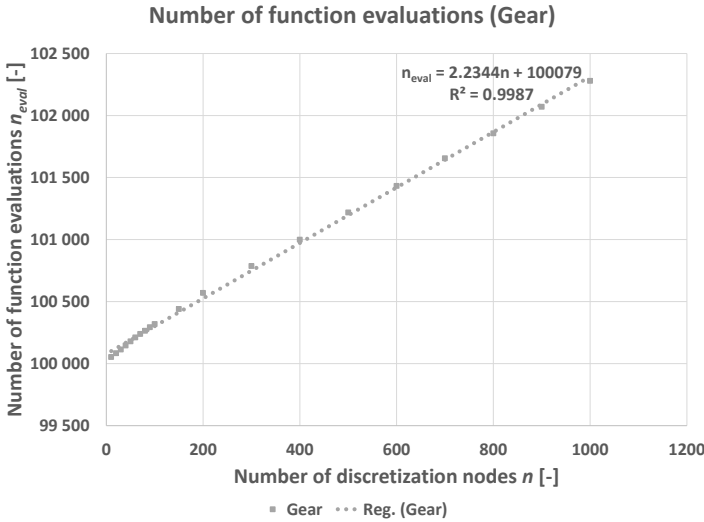

Figure 9. Number of temperature function evaluations in Gear's method.

On the other hand, Figure 10 presents a comparison of the number of multiplications depending on the number of discretization nodes.
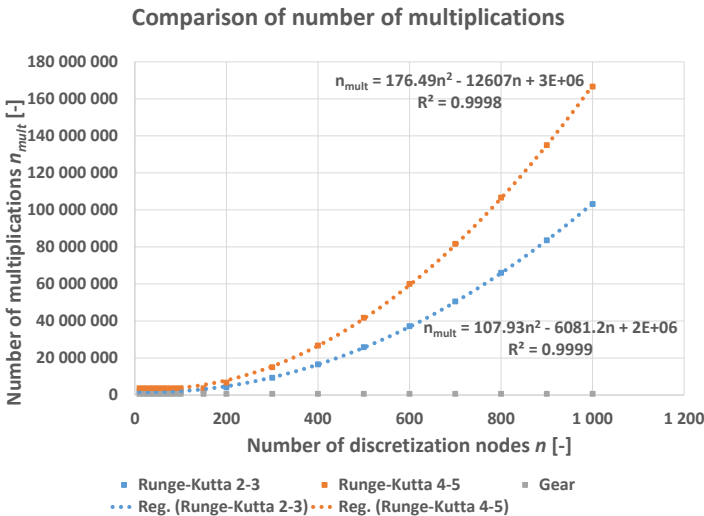

Figure 10. Comparison of the number of multiplications.

Similar to the previous case, the number of multiplications in Gear's method in relation to the number of discretization nodes is also presented separately in Figure 11.
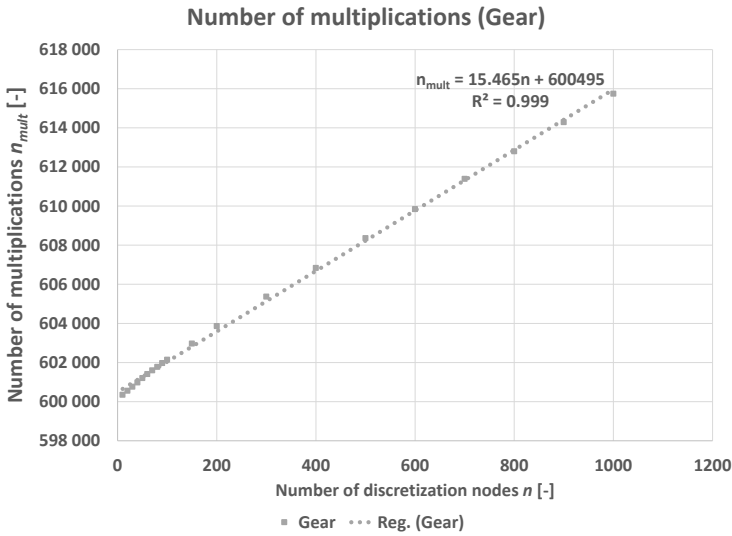
Number of multiplications (Gear)

$n_{mult} = 15.465n + 600495$
$R^2 = 0.999$

Number of multiplications n_{mult} [-]

Number of discretization nodes n [-]

■ Gear ···· Reg. (Gear)

Figure 11. Number of multiplications in Gear's method.

Moreover, the analogous comparison related to the number of summations has also been prepared and shown in Figure 12.
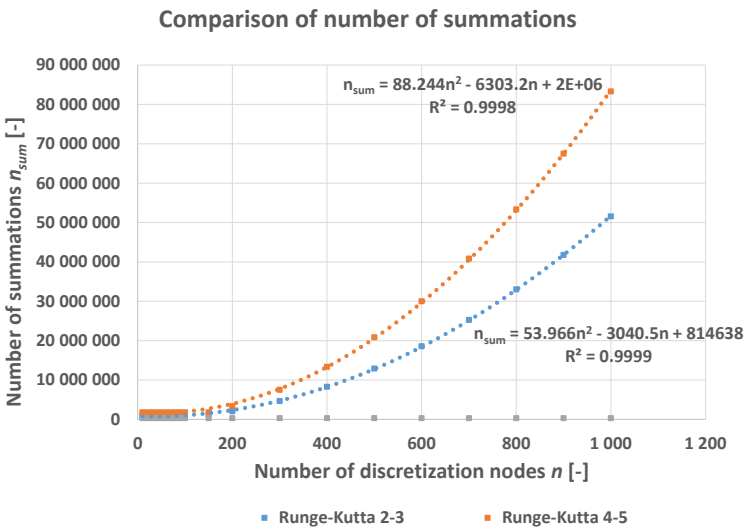
Comparison of number of summations

$n_{sum} = 88.244n^2 - 6303.2n + 2E{+}06$
$R^2 = 0.9998$

$n_{sum} = 53.966n^2 - 3040.5n + 814638$
$R^2 = 0.9999$

Number of summations n_{sum} [-]

Number of discretization nodes n [-]

■ Runge-Kutta 2-3   ■ Runge-Kutta 4-5

Figure 12. Comparison of the number of summations.

The number of summations in Gear's method, in turn, is presented in Figure 13.

Number of summations (Gear)
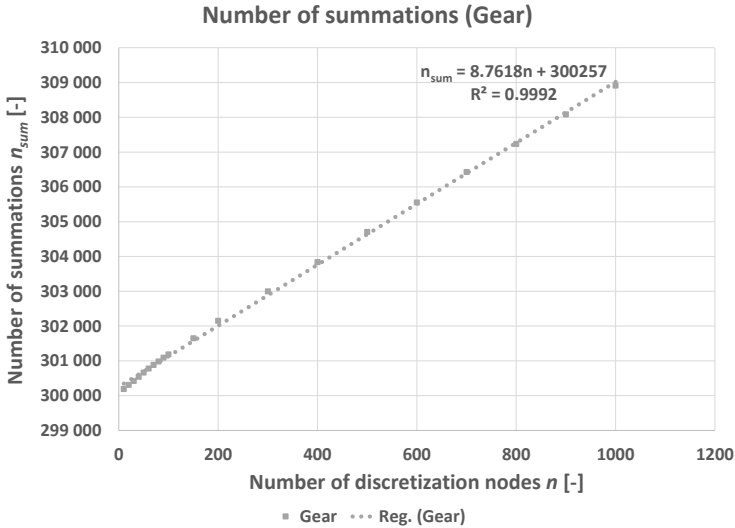
$$n_{sum} = 8.7618n + 300257$$
$$R^2 = 0.9992$$

Figure 13. Number of summations in Gear's method.

Analyzing the results presented in the figures above, it is clearly visible that the algorithms based on the Runge-Kutta formulas, marked as Runge-Kutta 2–3 (formula of the second and third order) and Runge-Kutta 4–5 (formula of the fourth and fifth order), are characterized by greater computational complexity than the algorithm using Gear's method, marked as Gear. The number of temperature function evaluations obtained using the Runge-Kutta methods is significantly greater than the analogous number of temperature function evaluations in Gear's method. A similar situation is observed for the number of multiplication and summation operations. In these cases, Gear's method demands a considerably smaller number of multiplications and summations than the Runge-Kutta algorithms. In the case of a medium number of discretization nodes (about 1000), the Runge-Kutta 2–3 method needs over 150 times more function evaluations, multiplications, and summations than Gear's method. On the other hand, the Runge-Kutta 4–5 method demands almost 300 times more operations than Gear's.

In the case of very big computational problems (for example, in the modeling of temperature distribution in realistic three-dimensional nanoelectronic structures where the number of discretization nodes exceeds 40 million), these differences are even more pronounced. This means that, in the case of an increased number of discretization nodes in the heat transfer problems described using the Dual-Phase-Lag equation in nanoelectronic structures, Gear's algorithm allows for the significant acceleration of computations in relation to the Runge-Kutta algorithms. A comparison of the measured and estimated computation times for all analyzed numerical meth-

ods for discretization mesh including 200, 1000, and 40 million nodes is presented in Table 1.

Table 1

Comparison of the estimated computation times for Runge-Kutta's and Gear's algorithms.

Method	Estimated computation times [s]		
	200 nodes	1000 nodes	40,000,000 nodes
Runge-Kutta 2–3	49.0731	2111.8464	$\sim 4.6 \cdot 10^{12}$
Runge-Kutta 4–5	80.5080	3209.6471	$\sim 7.0 \cdot 10^{12}$
Gear	48.5045	750.3439	$\sim 3.5 \cdot 10^{7}$

It is clearly visible that, for very big computational problems (40,000,000 nodes), the computation time in Gear's method can take about 1.1 year; in the Runge-Kutta 2–3 method – 145 865 years; and in the Runge-Kutta 4–5 method – a full 221,968 years (using the same computational node as in the presented research). However, three-dimensional problems may demand more time and a greater number of operations. This means that, for the analyzed problem, the computation time in the Gear's algorithm is even 200,000 times shorter than the computation time in the Runge-Kutta methods. Moreover, based on the data presented in Figures 7–13, it can be assumed that Gear's algorithm has time complexity $O(n)$, while the Runge- Kutta algorithms have time complexity $O(n^2)$.

It is also worth saying that, for a small number of discretization nodes, Gear's method demands a little bit longer time than the Runge-Kutta 2–3 method does. The inflection point is observed when the number of nodes is approximately equal to 100 (see Figure 15). This results mainly from the fact that, for a small number of nodes in Gear's method, the computational activity related to sparse matrix implementation is relatively large. With the increase of number of discretization nodes, this activity decreases in relation to all required computations.

Moreover, the convergence of the proposed algorithm has also been considered. In order to prove its convergence, relative error ε of the values of temperature was computed. This was obtained using the following expressions:

$$\varepsilon_k = \frac{T_k - T_{max_k}}{T_{max_k}} \qquad \text{for} \quad k = 10, \ldots, 1000, \tag{36}$$

where:

- T_k is the value of the temperature received for k nodes, where k=10, ..., 1000,
- T_{max_k} is the value of the temperature received for the maximum number k of nodes used in the simulation,
- ε_k is the value of the simulation error computed for k nodes, where k=10, ..., 1000.

Due to the fact that the algorithm based on Gear's method is characterized by the least computational complexity (as proven earlier), the relative error was computed

using the temperature distribution based on Gear's method. The relative errors for a chosen time value equal to 500 ps and different numbers of nodes are demonstrated in Figure 14.
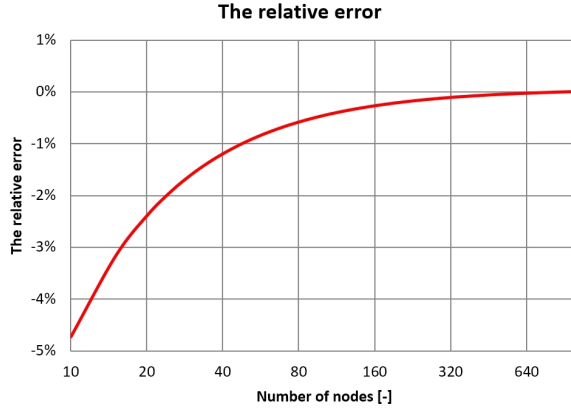

Figure 14. The relative error of the temperature value computation.

It is clearly seen that the relative error of the temperature value computation is reduced when the number of discretization nodes increases. This situation firmly indicates that the proposed algorithm based on the Dual- Phase-Lag equation is convergent. It is also worth saying that the number of the temperature function evaluation increases fast with a decrease in the relative error of the temperature value computation using Gear's method. This dependence is demonstrated in Figure 15.
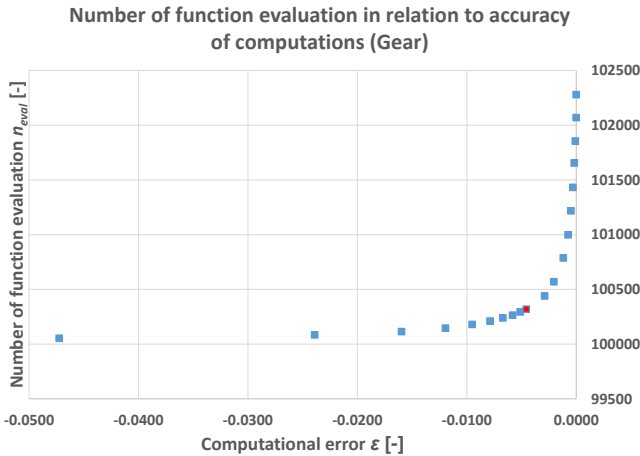

Figure 15. Comparison of the number of temperature function evaluations in relation to the relative error of temperature value computation. The red dot indicates the inflection point.

The accuracy, computation times, number of temperature function evaluations, number of multiplication and summation operations, and character of the relation presented in Figure 15 results mainly from the use of the predictor-corrector method in Gear's algorithm.

6. Conclusions

In this paper, the Dual-Phase-Lag model was employed to simulate the heat transfer in a nanosized solid state. The use of the mentioned model is dictated by its correctness in relation to the structures whose size do not exceed a few hundred nanometres.

In order to solve the Dual-Phase-Lag equation numerically, the Finite Difference Method was used. Moreover, some numerical methods for solving ordinary differential equations have been employed. One of the most-effective methods is based on Gear's method, and it gives the best results in the context of the lowest computational complexity problem. Furthermore, the research has shown that the solution using the proposed Finite Difference scheme is convergent; thus, it can be applied in solving thermal problems.

The numerical analysis of the computational complexity, presented in Chapter 5, is very important due to the necessity of practical solving of the realistic three-dimensional problems that may contain over 40 million mesh nodes. The presented analysis indicates that Gear's algorithm has linear time complexity while the Runge-Kutta algorithms have time complexity $O(n^2)$.

It is also worth emphasizing that this kind of research is an utterly new approach in solving the complex thermal problem in solid states.

Acknowledgements

References

[1] Antaki P.: Solution for non-Fourier dual phase lag heat conduction in a semiinfinite slab with surface heat flux. *International Journal of Heat and Mass Transfer*, vol. 41(14), pp. 2253–2258, 1998.

[2] Cahill D., Ford W., Goodson K., Mahan G., Majumdar A., Maris H., Merlin R., Phillpot S.: Nanoscale thermal transport. *Journal of Applied Physics*, vol. 93(2), pp. 793–818, 2003.

[3] Chen G.: Ballistic-diffusive equations for transient heat conduction from nano to macroscales. *Journal of Heat Transfer*, vol. 124(2), pp. 320–328, 2001.

[4] Fourier J.: *Theorie analytique de la chaleur*. Firmin Didot, Paris, 1988.

[5] Gutfeld R., Nethercot A.: Heat pulses in quartz and sapphire at low temperatures. *Physical Review Letters*, vol. 12(23), pp. 641–643, 1964.

[6] Hebboul S., Wolfe J.: Lattice dynamics of InSb from phonon imaging. *Zeitschrift für Physik B Condensed Matter*, vol. 73(4), pp. 437–466, 1989.

[7] Janicki M., Samson A., Raszkowski T., Zubert M., Napieralski A.: Comparison of Green's function solutions for different heat conduction models in electronic nanostructures. *Microelectronics Journal*, vol. 46(12A), pp. 1162–1166, 2015.

[8] Janicki M., Zubert M., Napieralski A.: Convergence of Green's function heat equation solutions in electronic nanostructures. *Proceedings of the 21st International Conference Mixed Design of Integrated Circuits and Systems*, pp. 285–288, 2014.

[9] Janicki M., Zubert M., Napieralski A.: Green's function solution of hyperbolic heat equation suitable for thermal analysis of electronic nanostructures. *Proceedings of 20th International Workshop on Thermal Investigations of ICs and Systems (THERMINIC)*, pp. 1–4, 2014.

[10] Janicki M., Zubert M., Samson A., Raszkowski T., Napieralski A.: Green's Function Solution for Dual-Phase-Lag Heat Conduction Model in Electric Nanostructures. *Proceedings of 31th Annual Semiconductor Thermal Measurement and Management Symposium (SEMI-THERM)*, pp. 95–98, 2015.

[11] Liu S., Xu X., Xie R., Zhang G., Li B.: Anomalous heat conduction and anomalous diffusion in low dimensional nanoscale systems. *The European Physical Journal B*, vol. 85(10: 337), 2012.

[12] Maudgal V.: Computer-aided thermal analysis. *Hybrid Circuit Technology*, pp. 19–21, 1991.

[13] Mochnacki B., Paruch M.: Cattaneo-Vernotte Equation. Identification of Relaxation Time Using Evolutionary Algorithms. *Journal of Applied Mathematics and Computational Mechanics*, vol. 12(4), pp. 97–102, 2013.

[14] Raszkowski T., Zubert M., Janicki M., Napieralski A.: Numerical solution of 1-D DPL heat transfer equation. *Proceedings of the 22nd International Conference Mixed Design of Integrated Circuits and Systems*, pp. 436–439, 2015.

[15] Tzou D.: A Unified Field Approach for Heat Conduction From Macro- to Micro-Scales. *Journal of Heat Transfer*, vol. 117(1), pp. 8–16, 1995.

[16] Xu M., Wang L.: Dual-phase-lagging heat conduction based on Boltzmann transport equation. *International Journal of Heat and Mass Transfer*, vol. 48 (25–26), pp. 5616–5624, 2005.

[17] Zubert M., Janicki M., Raszkowski T., Samson A., Nowak P., Pomorski K.: The Heat Transport in Nanoelectronic Devices and PDEs Translation into Hardware Description Languages. *Bulletin de la Société des Sciences et des Lettres de Łódź, Série: Recherches sur les Déformations*, vol. 64(3), pp. 69–80, 2014.

Affiliations

Tomasz Raszkowski
     Department of Microelectronics and Computer Science, Lodz University of Technology,
     ul. Wólczańska 221/223, 90-924, Łódź, Poland, `traszk@dmcs.p.lodz.pl`

Agnieszka Samson

Department of Microelectronics and Computer Science, Lodz University of Technology, ul. Wólczańska 221/223, 90-924, Łódź, Poland, `asamson@dmcs.p.lodz.pl`